Hindawi
Journal of Nanomaterials
Volume 2022, Article ID 1859698, 9 pages
https://doi.org/10.1155/2022/1859698

Research Article

Stability Analysis of Fe_3O_4-OA-MWCNT Nanocomposite-Based Nanofluid

Muhammad Nadeem,[1] **Sumbul Purree**,[1] **M. G. B. Ashiq**,[2] **and Hafiz Muhammad Ali**[3,4]

[1]*Department of Basic Sciences, University of Engineering and Technology, Taxila, 47056, Pakistan*
[2]*Department of Physics, College of Science, Imam Abdulrahman Bin Faisal University, P.O. Box 1982, Dammam 31441, Saudi Arabia*
[3]*Department of Mechanical Engineering, King Fahd University of Petroleum and Minerals, Dhahran 31261, Saudi Arabia*
[4]*Interdisciplinary Research Center for Renewable Energy and Power Systems (IRC-REPS), King Fahd University of Petroleum and Minerals, Dhahran 31261, Saudi Arabia*

Correspondence should be addressed to Muhammad Nadeem; nadeem.badani@uettaxila.edu.pk and Hafiz Muhammad Ali; hafiz.ali@kfupm.edu.sa

Received 21 March 2022; Revised 30 May 2022; Accepted 2 June 2022; Published 25 June 2022

Academic Editor: Ibrahim Alarifi

The aim of this project is to fabricate a highly stable Fe_3O_4-OA-MWCNT composite and its colloidal suspension in polyalphaolefin (PAO) base fluid for heat transfer applications. The nanocomposite was produced in three mass ratios (0.5 : 1, 1 : 1, and 1.5 : 1) to explore the concentration effects on the stability of the nanocomposite. XRD analysis and FTIR spectroscopy were conducted to inspect the phase and composition of the synthesized nanocomposite. The crystallite sizes (3.75 nm, 7.74 nm, and 7.52 nm) and dislocation densities of each composite were calculated, and it was revealed that the samples with high concentration of iron oxide nanoparticles showed small defects in their lattices. Dispersion stability of ferrofluids was also examined by natural deposition method for 365 days. The ferrofluids displayed high stability for more than one year with no sign of sedimentation. Thermal conductivity of the nanofluid was also measured via. A transient plane source method and a linear trend with slight deviation were observed.

1. Introduction

Ferrofluids, also known as ferromagnetic fluids, are an innovative class of nanofluids which comprises magnetic nanoparticles suspended into the base fluids like water, EG, and oil [1]. For the past decades, a lot of research has been done on these fluids which revealed that the ferrofluids are beneficial for heat transfer applications, i.e., oil recovery [2], heat exchanger [3], power generation [4], electronics cooling [5], and solar systems [6] because of their unique chemical, thermal, physical, mechanical, and magnetic properties [1]. These ferromagnetic nanomaterials embody maghemite (Fe_2O_3 or γ-Fe_2O_3), magnetite (Fe_3O_4), and ferrites composed of nickel (Ni), cobalt (Co), Manganese (Mn), silver (Ag), barium (Ba), lithium (Li), chromium (Cr), and zinc (Zn) [7].

The superparamagnetic behavior of ferrofluids corresponds to quick and firm response to relatively weak magnetic fields which make them easier to control magnetically [8]. However, the applications of these magnetic fluids have been restricted greatly due to them being heavy causing sedimentation and agglomeration which directly affects the heat transfer capability of nanofluids. This is because soft magnetic materials have very high apparent density value in comparison to other materials. Also, magnetic nanoparticles possess high chemical activity and are oxidized very easily. Such materials are coated with suitable polymers or surfactants, e.g., oleic acid, castor oil, and

sodium lauryl sulphate (SLS) in order to tackle the issue regarding the stability of ferrofluids [9]. Zareei et al. [10] fabricated alumina/water based nanofluid and used three surfactants sodium dodecyl sulphate (SDS), cetyl trimethyl ammonium bromide (CTAB), and Triton X-100 to investigate their effect on pH and particle size. Al-Waeli et al. [11] studied the influence of CTAB, SDS, tannic acid+ammonia, dodecyl benzene sulphonates (SDBS) and sodium deoxycholate on silica-based nanofluid. Chakraborty et al. [12] observed the effect of surfactants like SDS and Tween-20 on Cu-Zn-Al-based nanosuspension and reported 20.9% thermal conductivity with SDS as a surfactant. The choice of surfactants depends upon the types of base fluid. For polar fluids, water-soluble surfactants are used and, for nonpolar, the opposite [13]. Although surfactants reduce the apparent density to some extent, this method is still not considered to be highly effective as it also affects the thermal conductivity. Hence, synthesis of magnetic composites is thought to enhance the thermal efficiency and stability of these innovative fluids by reducing their apparent density [14]. For this purpose, carbon nanotubes are said to possess very small density, unique cylindrical structure, high mechanical strength, and great chemical stability and considered a good choice to reduce agglomeration and enhance the thermal conductivity of ferrofluids by researchers, scientists, and engineers [15–17]. Shi et al. [18] synthesized a superparamagnetic nanofluid using Fe_3O_4@CNT composite and studied the thermal conductivity via controlling the mass ratio of composite and magnetic field. Shahsavar et al. [19] examined heat transfer and entropy generation through natural convection of Fe_3O_4@CNT hybrid nanofluid inside a concentric horizontal annulus. Liu et al. [20] observed thermal conductivity of 24.25% and 22.62% when inquired Fe_3O_4@CNT nanocomposite in water based fluid for the effect of oscillating magnetic field. Saba and Ahmed et al. conducted an investigation on flow and heat transfer properties of Fe_3O_4@CNT/H_2O nanofluid inside a very long asymmetric channel with porous walls and declared that the CNT's dispersion in a nanofluid has a great influence on the transport properties. As mentioned above, several studies with open literature on Fe_3O_4-MWCNT have been reported with high thermal performance. However, nanofluid with Fe_3O_4/MWCNT composite and polyalphaolefin oil as a cooling agent have not been reported yet. PAO has been used in various industries as a lubricant and as a coolant [21]. Also, past literatures reported that nanofluids comprising insulating oil base fluids like PAO with poor heat transfer properties are more stable and homogeneous with high heat transfer rates [22]. In addition, the viscosity of PAO usually decreases with increase in temperature which has a significant effect on thermal conductivity [23, 24].

In this paper, the nanocomposite of Fe_3O_4 blended with multiwalled carbon nanotubes (MWCNT) with low apparent density and a hybrid nanofluid with base fluid of polyalphaolefin (PAO) is synthesized to explore a method to fabricate a highly stable nanofluid with high thermal conductivity for heat transfer application. Thermal conductivity of prepared nanofluid by controlling the morphology of nanoparticles, added volume fraction, minimizing agglomeration, and enhanced stability of the nanoparticles in the base fluid is also analyzed in this work.

2. Materials and Methods

2.1. Chemicals. All the chemicals, ferrous chloride ($FeCl_2$), ferric chloride ($FeCl_3$), ammonium hydroxide (NH_4OH), hydrochloric acid (HCl), deionized water, multiwalled carbon nanotubes (MWCNT), oleic acid, o-xylene, and polyalphaolefin (PAO), are acquired/purchased in Pakistan. All these reagents were analytical grade and were used without further purification.

2.2. Synthesis of Iron Oxide Nanoparticle. Iron oxide nanoparticles were prepared by a modified version of chemical coprecipitation method [25]. At first, ferrous chloride tetrahydrate and ferric chloride hexahydrate were dissolved in 100 ml of distilled water under constant stirring for 20 minutes. After that, the pH of this solution was maintained at 10 by adding 35 ml of ammonium hydroxide dropwise during constant stirring at 1100 rpm for 20 minutes. The solution slowly turned black indicating the formation of precipitates. These precipitates were collected via centrifugation at 4000 rpm for 10 minutes. Then, they were washed with distilled water 4-5 times and dried at 40°C in oven overnight.

2.3. Coating of Iron Oxide Nanoparticles with Oleic Acid. The synthesized iron oxide nanoparticles were coated with oleic acid to reduce the apparent density of nanoparticles. For this, 2 wt.% of Fe_3O_4 nanoparticles was added into the 10% (*v*/*v*) oleic acid solution during constant stirring at 400 rpm at 40°C for 1 hour. The obtained viscous solution was centrifuged at 4000 rpm to collect the nanoparticles. These nanoparticles then washed with alcohol 3-4 times and were dried in an oven for 24 hours.

2.4. Nanocomposite Fabrication. A solution mixing method was used to fabricate the multiwalled carbon nanotubes (MWCNT) based nanocomposite. For this purpose, iron oxide nanoparticles were mixed with MWCNT in three different mass ratios of 0.5 : 1, 1 : 1, and 1.5 : 1 in 50 ml oleic acid solution during rigorous stirring for 1100 rpm at 40°C temperature for 1 hour. The MWCNT were added into the solution during second half, and the solution was sonicated for 2 hours at the same temperature. Residuals were removed through ethanol for several times. Then, obtained composites were dried in oven for a day and grounded to powder form for further proceedings.

2.5. Synthesis of Hybrid Nanofluid. Prepared Fe_3O_4-OA-MWCNT nanocomposites with three different compositional mass ratios of 0.5 : 1, 1 : 1, and 1.5 : 1 were used to create polyalphaolefin-based hybrid nanofluid. Nanofluids were prepared in three different volume fractions of 0.3 wt.%, 0.5 wt.%, and 0.7 wt.% for each composite. Based on known weights and densities of the sample, the required

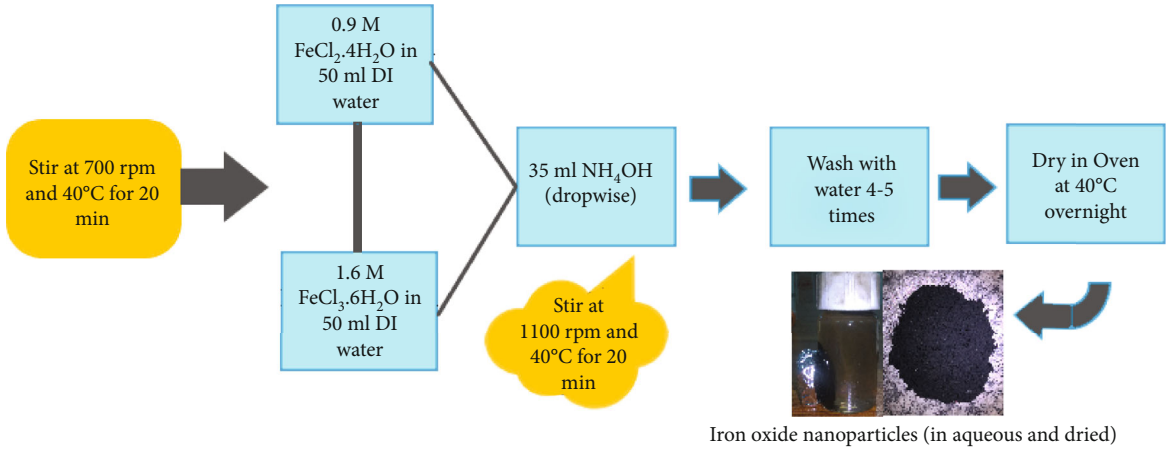

Figure 1: Flow diagram of synthesis of IONPs.

volume fraction of nanocomposite was predicted by following equation:

$$\phi = \frac{\left(W_{\text{Nanocomposite}}/\rho_{\text{Nanocomposite}}\right)}{\left[\left(W_{\text{Nanocomposite}}/\rho_{\text{Nanocomposite}}\right) + \left(W_{\text{Polyalphaolefin}}/\rho_{\text{Polyalphaolefin}}\right)\right]} \times 100. \quad (1)$$

Then nanocomposites were dispersed in 14 ml of polyalphaolefin oil through sonication of 2 hours at 70°C to obtain a stable suspension (see Figure 1).

3. Characterization

Crystal behavior and phase identification were analyzed via XRD analysis. An X-ray diffractometer of D8 Advance (Bruker Germany) (LYNX EYE linear detector) and a diffractometer equipped with copper tube ($\lambda = 1.5406A$) were used for the measurements with an average range of 20° to 80° along with the step size of 0.5. 6300 type A Jasco infrared spectrometer (4 cm^{-1} resolution with a scanning speed of 2 mm/sec) was used to record the complex spectrum of synthesized nanocomposite. The spectral range of 399.193 to 4000 cm^{-1} was used for the compositional analysis of the sample at room temperature. Surface morphology of synthesized pure iron oxide nanoparticles was analyzed via. A JEM-2100 transmission electron microscope (TEM) with 200 kV accelerating voltage was used. Sedimentation photograph technique was used to observe the stability of Fe_3O_4-OA-MWCNT amalgam in polyalphaolefin (PAO) base fluid. It works on the principle that the size of nanocomposite is directly related to the stability of particles in the nanofluid as particle with large size will settle down quickly on the bottom of the container. For this, nanocomposites with mass ratios of 0.5 : 1, 1 : 1, and 1.5 : 1 of IONPs : MWCNT were used to prepare nanofluids of three different volume fractions (i.e.,0.3 wt.%, 0.5 wt.%, and 0.7 wt.%). The photographs were taken at various intervals with maximum after one year. Hot Disc TPS 2500 Thermal Constant Analyzer, which employ transient plane source method, with thermal conductivity range of 0.005 to 1800 Wm/K, and can accommodate the temperature from cryogenic to 1000°C, was used to obtain the heat transfer data of each composition with uncertainty error of 2% to 5%. A thermal conducting plane

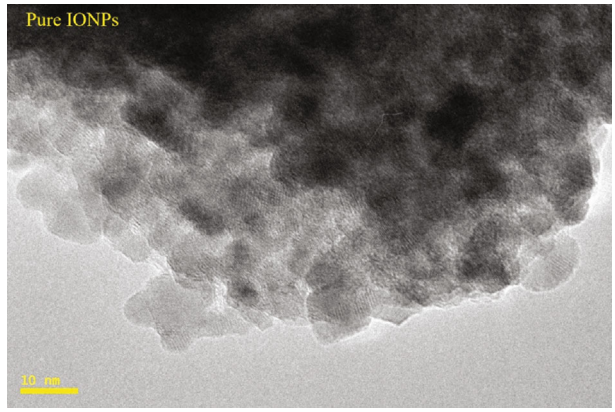

Figure 2: TEM image of pure Fe_3O_4 nanoparticles.

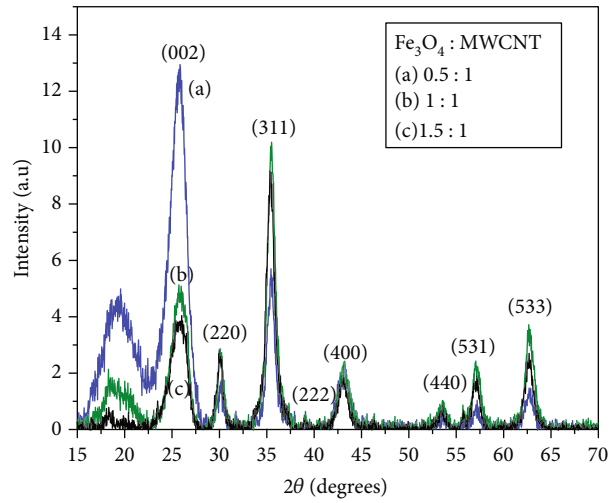

Figure 3: XRD spectra of Fe_3O_4-OA-MWCNT nanocomposite with mass ratios between Fe_3O_4 : MWCNT, i.e., (a) 0.5 : 1, (b) 1 : 1, and (c) 1.5 : 1.

sensor acting as a heat source is placed between two testing sample. The rise in temperature of the source enhances the heat dissipation of the material under examination at a rate that depends on its thermal transport properties. The sample was sonicated at 40°C for 1 hour for homogeneity and then was placed into holders. Thermal transport properties were measured at pr. depth of approx. 1.6 mm of the sample. The equipment was calibrated three times before calculation with standard fluid (PAO) in this case. About five measurements at temperature of 0-100°C were taken for about 4 hours with 25°C intervals in between measurements. The process was repeated several times to ensure the validity of the results.

4. Results and Discussion

Three different samples of Fe_3O_4-OA-MWCNT nanocomposite having compositional ratios: (a) 0.5 : 1 (S1), (b) 1 : 1 (S2), and (c) 1.5 : 1 (S3), between IONPs and MWCNT have been synthesized to investigate its phase, crystal structure, and chemical composition using various techniques like XRD and FTIR. Nanofluids with volume concentration 0.3 wt.%, 0.5 wt.%, and 0.7 wt.% for each sample have also been prepared under suitable conditions to explore its dispersion stability.

4.1. Surface Morphology of IONPs. The stability of nanofluids is directly influenced by the nature of nanoparticles [26]. Therefore, surface morphology and agglomeration behavior of iron oxide nanoparticles were examined in detail using a transmission electron microscope (TEM). Figure 2 clearly confirms the spherical shape and crystalline nature of the pure IONPs. The particles show agglomeration even after sonication of 2 hours in the ethanol (solvent). This is due to the magnetic and inner particle interaction among of Fe_3O_4 nanoparticles. The clusters were formed due to high surface charge and dipolar interactions of particles.

4.2. Phase and Crystal Structure. Figure 3 (a–d) contains the XRD pattern of all samples, i.e., S1, S2, and S3. The reflecting planes (220), (311), (222), (400), (440), (511), (531), and (533) corresponding to 2θ angles 30°, 35.5°, 38°, 43°, 53.7°, 53.4°, 57.3°, and 62.8° show the characteristic peaks of iron oxide nanoparticles. The lack of planes (210), (300), and (320) proves the absence of maghemite phase when compared to JCPD card No. 19-0629, as the obtained peaks match with the standard peaks [27]. The lattice plane (002) at 25.95° of angle 2θ corresponds to the presence of interlayer stacking of graphene sheets embedded together and confirms the multiwalled nature of carbon nanotubes which matches exactly to the JCPD card No. 41-1487 confirming the existence of nanocomposite [28]. Comparing these peaks leads to conclusion that increasing the iron oxide ratio directly affects the crystallinity of the nanocomposite; i.e., the sharpness of peaks has been enhanced.

The crystallite size of nanocomposite was calculated using mostly used the Debye-Scherrer formula from the XRD pattern along with dislocation densities [29]:

$$D_{hkl} = \frac{0.94\lambda}{\beta \cos\theta}, \tag{2}$$

where D_{hkl}, β, λ, and θ corresponds to crystallite size, full wave half maximum, wavelength of Cu-k_α, and diffraction angle, respectively. The dislocation density (δ) is the measure of number of distortions/defects present in a crystal structure and is expressed in lines per square meter. It was also calculated by the following formula:

$$\delta = \frac{1}{D_{hkl}^{\,2}}. \tag{3}$$

Table 1 shows the value of diffraction angle, full wave half maximum (FWHM) in radians, crystallite size, and dislocation density of Fe_3O_4-OA-MWCNT nanocomposite with different mass ratios. Among all three nanocomposites, the one with least iron oxide content has the smallest size of 3.75 nm and increasing the magnetic content resulted in increase in crystallite size and decrease in defects. The maximum crystallite size observed is 7.52 nm of Fe_3O_4 : MWCNT with 1.5 : 1 mass ratios and the smallest dislocation density of 1.77×10^{16} lines/m^2. This is because oxidation or structural interactions due to hydroxyl or

Table 1: XRD parameters of Fe_3O_4-OA-MWCNT.

Fe_3O_4 : MWCNT	θ (degrees)	FWHM (radians)	Crystallite size (nm)	Dislocation density ($\times 10^{16}$) (lines/m^2)
0.5 : 1	25.96	0.03864	3.75	7.12
1 : 1	38.00	0.01871	7.74	1.67
1.5 : 1	35.38	0.01927	7.52	1.77

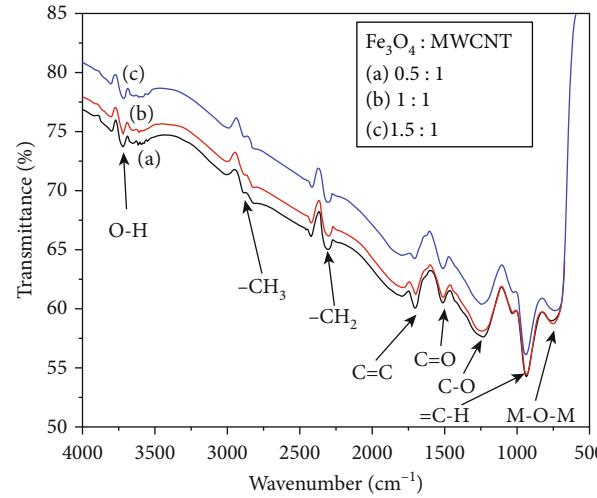

Figure 4: FTIR spectra of Fe_3O_4-OA-MWCNT nanocomposite with mass ratios between Fe_3O_4 : MWCNT, i.e., (a) 0.5 : 1, (b) 1 : 1, and (c) 1.5 : 1.

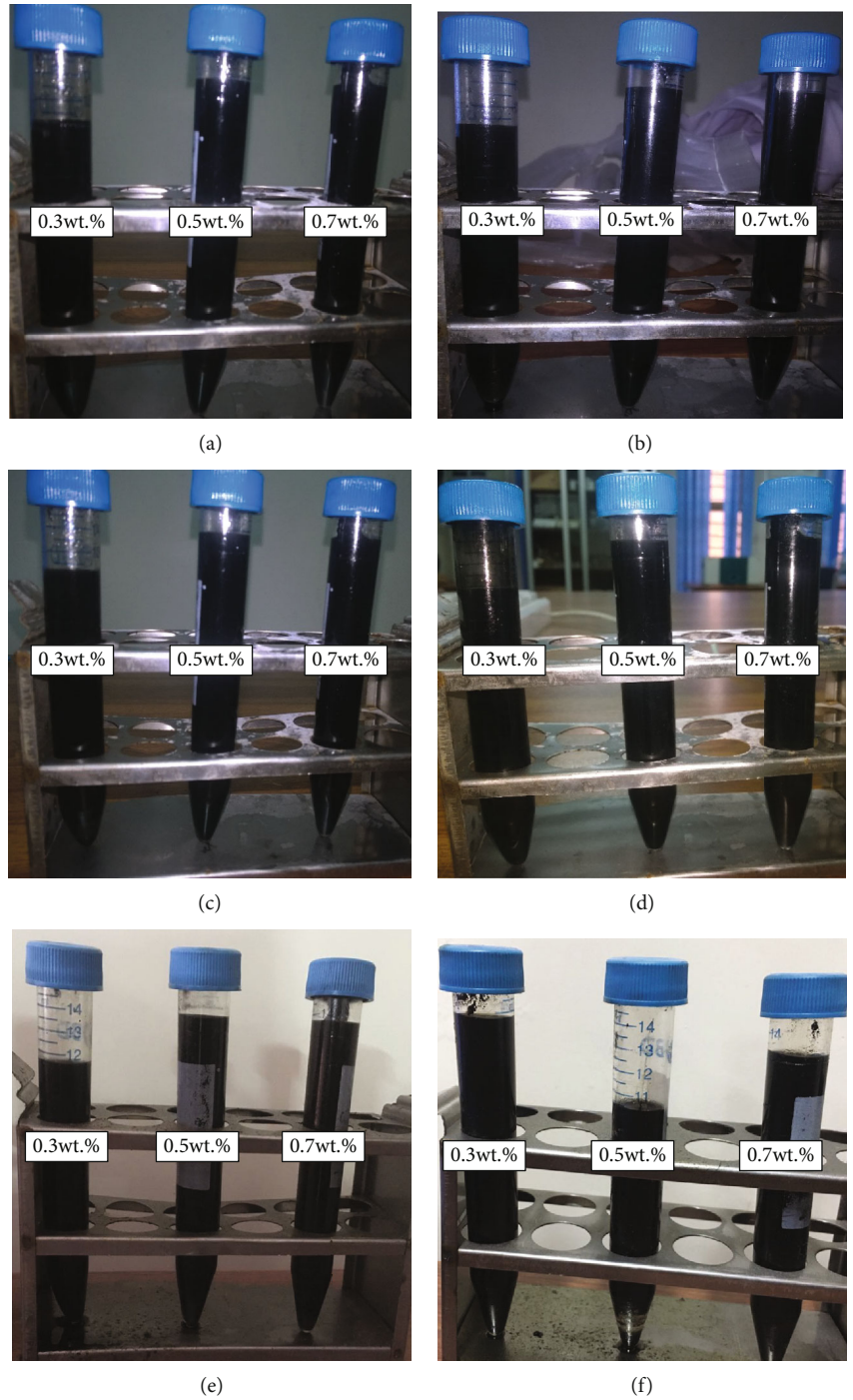

FIGURE 5: Nanofluid containing S1 (Fe_3O_4-OA-MWCNT)/PAO with weight of 0.3 wt.%, 0.5 wt.%, and 0.7 wt.% (2-hour sonication) after (a) one week, (b) one month, (c) four months, (d) six months, (e) eight months, and (f) one year.

carboxyl functional group affects the stacking of tubules causing distortions among the crystal lattices.

4.3. Compositional Analysis. Figure 4 shows the FTIR spectra of Fe_3O_4-OA-MWCNT nanocomposite with three different mass ratios (0.5 : 1, 1 : 1, and 1.5 : 1) of iron oxide and multi-walled carbon nanotubes. The wide absorption band at 929.92 cm^{-1} is due to the out of plane bending of =C-H bond. A broad band at 740.63 cm^{-1} in fingerprint region represents the stretching vibrations of Fe-O bond which shows slight deviations (747.36 cm^{-1} and 754.92 cm^{-1}) due to increase in the mass ratio of iron oxide nanoparticles in the composite. These absorption bands confirm the presence of metallic oxide nanoparticles. The presence of C=C was revealed by the absorption spectra at 1505.41-1695.55 cm^{-1} which indicates the hexagonal structure of the MWCNT.

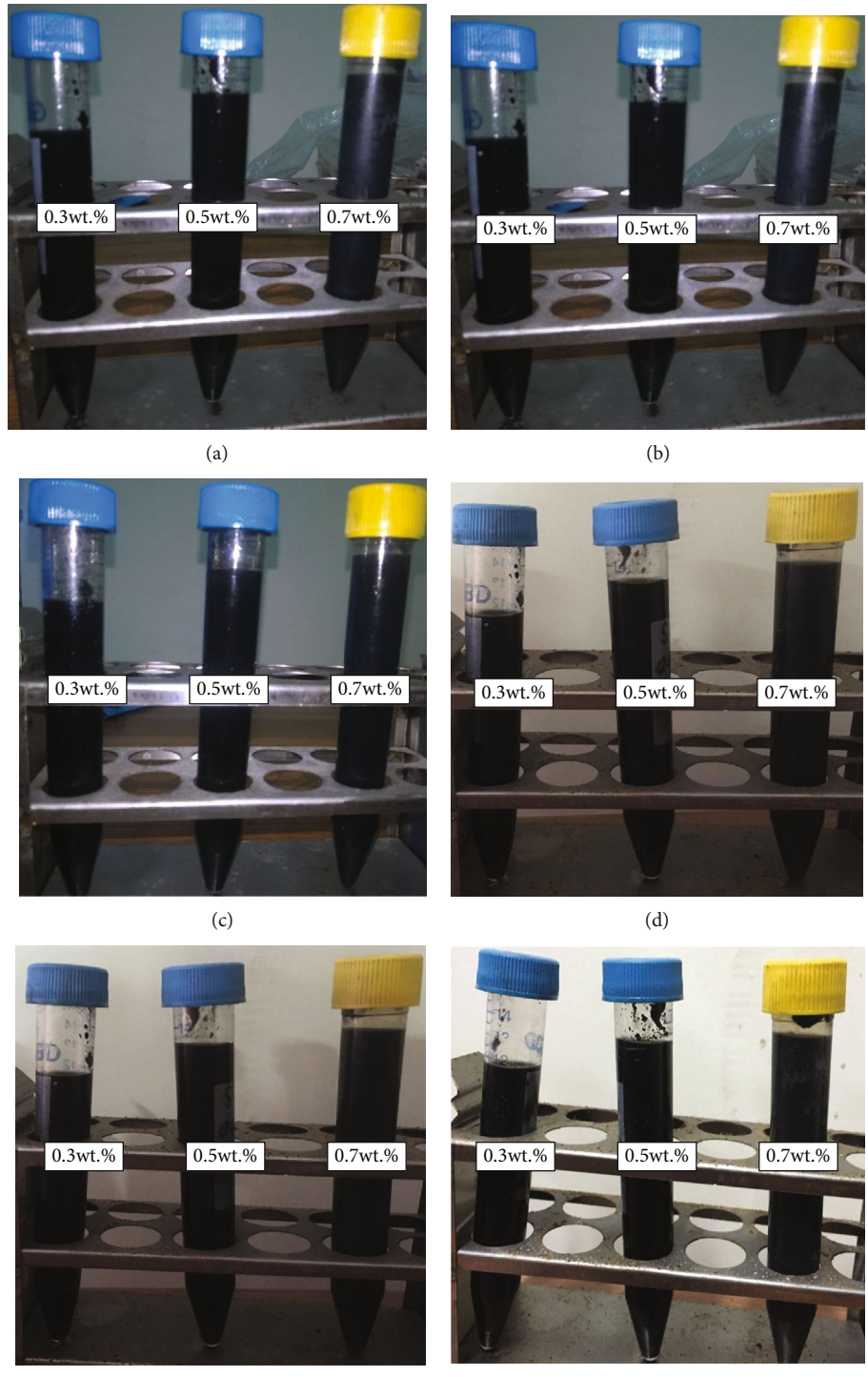

FIGURE 6: Nanofluid containing S2 (Fe_3O_4-OA-MWCNT)/PAO with weight of 0.3 wt.%, 0.5 wt.%, and 0.7 wt.% (2-hour sonication) after (a) one week, (b) one month, (c) four months, (d) six months, (e) eight months, and (f) one year.

The MWCNT shows very weak peaks of C=C aromatic ring stretching around 1600 cm^{-1} which is the indication of a large number of asymmetrical carbons present [30]. The absorption peaks at 1687.98 and 1512.98 cm^{-1} elucidate the presence of C=O. At 1050 cm^{-1}, a strong absorption peak from C-O bond stretching is obtained. The weak absorption peaks at 2313-2847 cm^{-1} indicate the presence of asymmetrical stretching of aromatic bonds of $-CH_2$ and $-CH_3$ which is due to alkyl groups at 3717.31 cm^{-1} shows the presence of O-H stretching vibrations which indicates the modification of MWCNT. Negligible intensity of O-H peak is the evidence that the prepared nanocomposite is hydrophobic in nature.

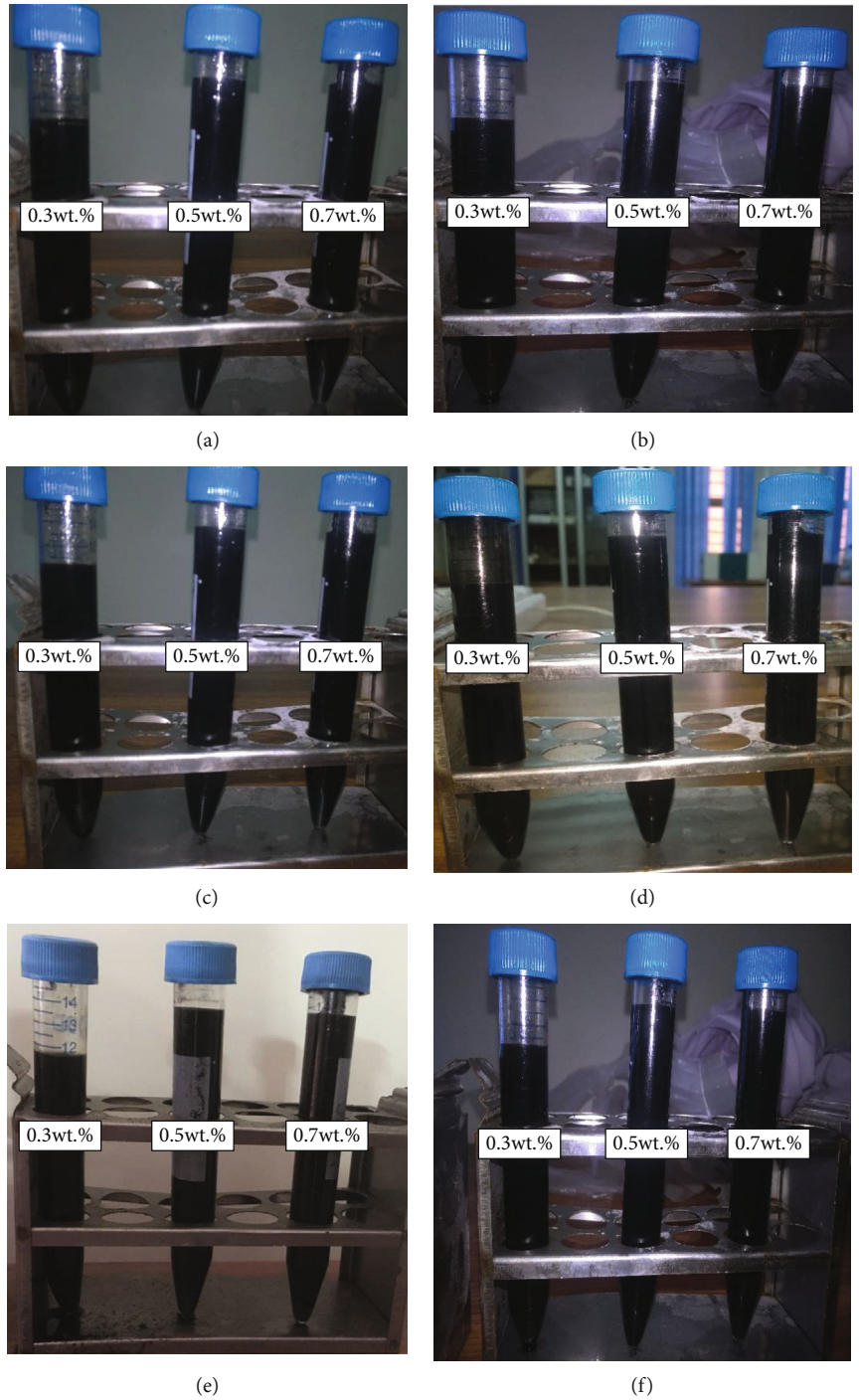

FIGURE 7: Nanofluid containing S3 (Fe_3O_4-OA-MWCNT)/PAO with weight of 0.3 wt.%, 0.5 wt.%, and 0.7 wt.% (2-hour sonication) after (a) one week, (b) one month, (c) four months, (d) six months, (e) eight months, and (f) one year.

4.4. Dispersion Stability. Dispersion stability is the most debated and important characteristics of nanofluids for thermal applications. The prepared samples were utilized to observe their aggregation behavior in the polyalphaolefin oil with respect to time. Figure 5 illustrates the stability investigation of polyalphaolefin oil containing sample S1 in three different volume fractions. It is evident in the figure that the ferrofluids comprising of S1 nanocomposite are stable after 12 months and negligible sedimentation was observed after six months.

Figure 6 shows the stability of sample S2-based nanofluids with respect to time. No apparent change in the color of suspension was observed even after 12 months indicating its high storage life.

Figure 7 reveals the dispersion behavior of colloids containing sample S3. After 12 months, suspensions showed

very high stability with negligible deposition due to presence of multiwalled carbon nanotubes (MWCNT) which form a complex three-dimensional structure making sedimentation difficult.

4.5. Thermal Conductivity. Thermal conductivity of polyalphaolefin oil-based nanofluid comprising of Fe_3O_4/OA/MWCNT nanocomposite was carefully calculated via a thermal constant analyzer at five different temperature values with 25°C interval among each value. The equipment was standardized using polyalphaolefin oil, and every calculation was repeated three times to ensure the reliability of the calculations.

Figure 8 shows the temperature dependence of the thermal conductivity at various volume fractions for PAO-based hybrid nanofluid measured at temperatures from 0°C to 100°C. It can be observed that the thermal conductivity diminishes with the increase in temperature, and a wide variation is observed at elevated temperature. Deviations in thermal conductivity curves were observed when compared to pure polyalphaolefin oil; i.e., Curve (d) shows rise in thermal behavior, and curve (c) shows reduction in thermal conductivity at high temperatures. This is due to rise in particle interactions which results in the formation of aggregates because of large aggregation time and sharp rise in temperature. This provides new pathways for heat transport, but when the aggregation is very high, it disrupts the thermal transport mechanism causing in the reduction of thermal conductivity, though the heat transfer reduces when temperature is enhanced but the thermal conductivity curve shift towards higher values when the particle concentration is increased. As observed in the above graph, the higher value of thermal conductivity was observed at a volume concentration of 0.7 wt.% and the lowest thermal conductivity was observed at 0.5 wt.% which is almost the same as pure polyalphaolefin oil. The rise of thermal conductivity observed due to the addition of nanocomposite in PAO was also calculated with its heat transfer rates varying from 0.25% to 0.9% as compared to base fluid which is not very high because of large cluster formation and poor heat transfer capacity of the oil. In the incompetent thermal performance of heat transfer fluids, energy loss is observed. This can be prevented with a lubricant consisting of good heat transfer capacity.

5. Conclusion

Fe_3O_4-OA-MWCNT nanocomposite with weight ratios of 0.5 : 1, 1 : 1, and 1.5 : 1 was magnificently synthesized via solution blend approach of in situ polymerization method, and its ferrofluids were prepared in polyalphaolefin oil with volume fractions, i.e., 0.3 wt.%, 0.5 wt.%, and 0.7 wt.% in the present study. The crystallite sizes of each composition of the sample (S1—0.5 : 1, S2—1 : 1, and S3—1.5 : 1) were carefully calculated (i.e., 3.75 nm, 7.74 nm, and 7.52 nm) using Scherrer's equation with dislocation densities 7.12×10^{16} lines/m^2, 1.67×10^{16} lines/m^2, and 1.77×10^{16} lines/m^2, accordingly. XRD analysis verified the crystal behavior of the nanocomposite while FTIR spectra confirmed the

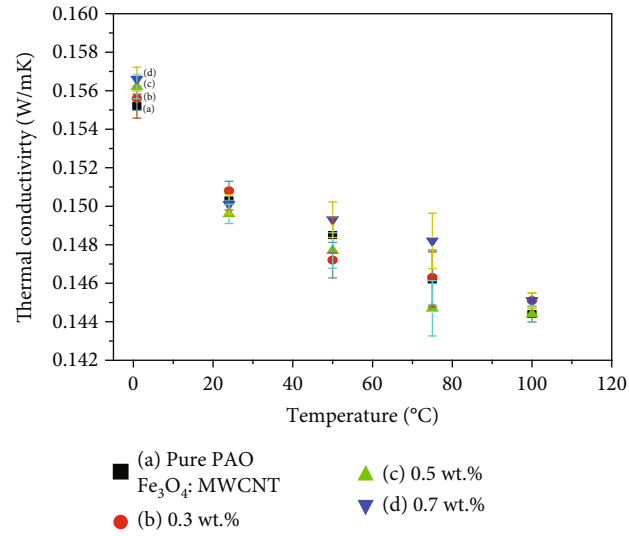

Figure 8: Thermal conductivity trend of Fe_3O_4/MWCNT/PAO nanofluid as a function of temperature. The error bars indicate the standard deviation of the values.

hydrophilic nature and formation of nanocomposite. The stability assessment revealed that each composition showed high aggregation stability and no apparent deposition was observed even after one year. The thermal conductivity of the sample determination showed the linear trend as a function of temperature and volume fraction, and highest thermal conductivity was observed for 0.7 wt.% at 50°C temperature when compared to pure PAO oil. This shows that Fe_3O_4-OA-MWCNT/PAO-based nanofluids have great potential for thermal applications as a lubricant and as a heat exchanger.

Data Availability

Data will be provided on reasonable request.

Conflicts of Interest

The authors declare that they have no conflicts of interest.

References

[1] M. Imran, A. H. Shaik, A. R. Ansari et al., "Synthesis of highly stable γ-Fe_2O_3ferrofluid dispersed in liquid paraffin, motor oil and sunflower oil for heat transfer applications," *RSC Advances*, vol. 8, no. 25, pp. 13970–13975, 2018.

[2] M. Ramezanpour and M. Siavashi, "Application of SiO $_2$–water nanofluid to enhance oil recovery," *Journal of Thermal Analysis and Calorimetry*, vol. 135, no. 1, pp. 565–580, 2019.

[3] M. U. Sajid and H. M. Ali, "Recent advances in application of nanofluids in heat transfer devices: a critical review," *Renewable and Sustainable Energy Reviews*, vol. 103, pp. 556–592, 2019.

[4] P.-H. Yen and J.-C. Wang, "Power generation and electric charge density with temperature effect of alumina nanofluids using dimensional analysis," *Energy Conversion and Management*, vol. 186, pp. 546–555, 2019.

[5] M. Bahiraei, S. Heshmatian, M. Goodarzi, and H. Moayedi, "CFD analysis of employing a novel ecofriendly nanofluid in a miniature pin fin heat sink for cooling of electronic components: effect of different configurations," *Advanced Powder Technology*, vol. 30, no. 11, pp. 2503–2516, 2019.

[6] H. Olia, M. Torabi, M. Bahiraei, M. H. Ahmadi, M. Goodarzi, and M. R. Safaei, "Application of nanofluids in thermal performance enhancement of parabolic trough solar collector: state-of-the-art," *Applied Sciences*, vol. 9, no. 3, p. 463, 2019.

[7] V. Singh, A. Kumar, M. Alam, A. Kumar, P. Kumar, and V. Goyat, "A study of morphology, UV measurements and zeta potential of zinc ferrite and Al_2O_3 nanofluids," *Materials Today: Proceedings*, vol. 59, pp. 1034–1039, 2022.

[8] X. Zhang, L. Sun, Y. Yu, and Y. Zhao, "Flexible ferrofluids: design and applications," *Advanced Materials*, vol. 31, no. 51, p. 1903497, 2019.

[9] H. Pu and F. Jiang, "Towards high sedimentation stability: magnetorheological fluids based on CNT/Fe_3O_4nanocomposites," *Nanotechnology*, vol. 16, no. 9, pp. 1486–1489, 2005.

[10] M. Zareei, H. Yoozbashizadeh, and H. R. M. Hosseini, "Investigating the effects of pH, surfactant and ionic strength on the stability of alumina/water nanofluids using DLVO theory," *Journal of Thermal Analysis and Calorimetry*, vol. 135, no. 2, pp. 1185–1196, 2019.

[11] A. H. A. Al-Waeli, M. T. Chaichan, H. A. Kazem, and K. Sopian, "Evaluation and analysis of nanofluid and surfactant impact on photovoltaic- thermal systems," *Case Studies in Thermal Engineering*, vol. 13, article 100392, 2019.

[12] S. Chakraborty, I. Sengupta, I. Sarkar, S. K. Pal, and S. Chakraborty, "Effect of surfactant on thermo-physical properties and spray cooling heat transfer performance of Cu-Zn-Al LDH nanofluid," *Applied Clay Science*, vol. 168, pp. 43–55, 2019.

[13] C. Scherer and A. M. Figueiredo Neto, "Ferrofluids: properties and applications," *Brazilian Journal of Physics*, vol. 35, no. 3A, pp. 718–727, 2005.

[14] L. Shi, Y. He, Y. Hu, and X. Wang, "Thermophysical properties of Fe_3O_4@CNT nanofluid and controllable heat transfer performance under magnetic field," *Energy Conversion and Management*, vol. 177, pp. 249–257, 2018.

[15] A. A. Nadooshan, H. Eshgarf, and M. Afrand, "Measuring the viscosity of Fe_3O_4-MWCNTs/EG hybrid nanofluid for evaluation of thermal efficiency: Newtonian and non-Newtonian behavior," *Journal of Molecular Liquids*, vol. 253, pp. 169–177, 2018.

[16] R. Nasrin, N. A. Rahim, H. Fayaz, and M. Hasanuzzaman, "Water/MWCNT nanofluid based cooling system of PVT: experimental and numerical research," *Renewable Energy*, vol. 121, pp. 286–300, 2018.

[17] M. H. Esfe, S. Esfandeh, M. K. Amiri, and M. Afrand, "A novel applicable experimental study on the thermal behavior of SWCNTs(60%)-MgO(40%)/EG hybrid nanofluid by focusing on the thermal conductivity," *Powder Technology*, vol. 342, pp. 998–1007, 2019.

[18] L. Shi, Y. He, Y. Hu, and X. Wang, "Controllable natural convection in a rectangular enclosure filled with Fe_3O_4@CNT nanofluids," *International Journal of Heat and Mass Transfer*, vol. 140, pp. 399–409, 2019.

[19] A. Shahsavar, P. Talebizadeh Sardari, and D. Toghraie, "Free convection heat transfer and entropy generation analysis of water-Fe_3O_4/CNT hybrid nanofluid in a concentric annulus," *International Journal of Numerical Methods for Heat & Fluid Flow*, vol. 29, no. 3, pp. 915–934, 2019.

[20] W. Liu, J. Alsarraf, A. Shahsavar, M. Rostamzadeh, M. Afrand, and T. K. Nguyen, "Impact of oscillating magnetic field on the thermal-conductivity of water- Fe_3O_4 and water- Fe_3O_4/CNT ferro-fluids: Experimental study," *Journal of Magnetism and Magnetic Materials*, vol. 484, pp. 258–265, 2019.

[21] X. Li, F. Yuan, W. Tian et al., "Heat transfer enhancement of nanofluids with non-spherical nanoparticles: a review," *Applied Sciences*, vol. 12, no. 9, p. 4767, 2022.

[22] S. N. Suhaimi, A. R. A. Rahman, M. F. M. Din, M. Z. Hassan, M. T. Ishak, and M. T. . Jusoh, "A review on oil-based nanofluid as next-generation insulation for transformer application," *Journal of Nanomaterials*, vol. 2020, 17 pages, 2020.

[23] A. K. Sleiti, "Heat transfer measurements of polyalpha-olefin-boron nitride nanofluids for thermal management and lubrication applications," *Case Studies in Thermal Engineering*, vol. 22, article 100776, 2020.

[24] S. Purree, M. Nadeem, M. Zubair et al., "Volume fraction effects on thermophysical properties of Fe $_3$ O $_4$/MWCNT based hybrid nanofluid," *International Journal of Nanoelectronics & Materials*, vol. 14, no. 1, 2021.

[25] M. Nadeem, "Synthesis of iron oxide nanoparticles for the anti cancer drugs delivery," *Universiti Teknologi Malaysia*, 2016.

[26] T. Le Ba, O. Mahian, S. Wongwises, and I. M. Szilágyi, "Review on the recent progress in the preparation and stability of graphene-based nanofluids," *Journal of Thermal Analysis and Calorimetry*, vol. 142, pp. 1–28, 2020.

[27] Y. Y. Byong and S. S. Kwak, "Assembly of magnetite nanoparticles into spherical mesoporous aggregates with a 3-D wormhole-like porous structure," *Journal of Materials Chemistry*, vol. 20, pp. 1–9, 2010.

[28] H. Xiong, L. Wang, S. U. Rehman et al., "Carbon coated core-shell FeSiCr/Fe_3C embedded in carbon nanosheets network nanocomposites for improving microwave absorption performance," *Nano*, vol. 15, no. 7, p. 2050094, 2020.

[29] H. Khan, A. S. Yerramilli, A. D'Oliveira, T. L. Alford, D. C. Boffito, and G. S. Patience, "Experimental methods in chemical engineering: X-ray diffraction spectroscopy—XRD," *The Canadian Journal of Chemical Engineering*, vol. 98, no. 6, pp. 1255–1266, 2020.

[30] R. Yudianti, H. Onggo, Y. Saito, T. Iwata, and J. I. Azuma, "Analysis of functional group sited on multi-wall carbon nanotube surface," *The Open Materials Science Journal*, vol. 5, no. 1, pp. 242–247, 2011.